Mixing of viscous immiscible liquids. Part 1: Computational models for strong–weak and continuous flow systems

P. DeRoussel[a], D.V. Khakhar[b], J.M. Ottino[a, *]

[a] Department of Chemical Engineering, Robert McCormick School of Engineering, Northwestern University, 2145 Sheridan Road, Evanston, IL 60208-3120, USA
[b] Department of Chemical Engineering, Indian Institute of Technology—Bombay, Powai, Bombay 400076, India

Abstract

Initial mixing of viscous immiscible liquids occurs by stretching and folding of large blobs on a global scale; later stages are controlled by repeated stretching, folding, breakup, and coalescence of individual filaments or drops at local or homogeneous flow scales. There is little hope of accounting for every detail as the mixing process evolves from the initial to final stages. Two models are presented: the first model (Mixing I) is suited for batch systems where decomposition into weak and strong flow regions is appropriate; the second model (Mixing II) is suited for continuous flow systems and is intended to be used in conjunction with a fluid mechanical model of the flow. The models presented here use only the most important physics of the local processes while making a connection between the overall global flow and the local dominated processes. The models calculate changes in morphology or drop size distribution due to changes in material and process parameters. Two aspects previously ignored are highlighted: formation of satellite drops upon breakup and distributions of stretching leading to wide distributions of length scales. Similar trends are obtained for both Mixing I and Mixing II models.

Results indicate that there is an exponential decrease in the volume average size with time (or distance along the mixer in the case of a continuous mixer). The average drop size decreases with increase in drop viscosity or the dispersed phase viscosity and with decrease in the interfacial tension. These results are in qualitative agreement with experimental data. The effect of reorientations in the continuous mixer is found to accelerate the rate of dispersion, and about five reorientations is found to be optimal. The spatial distribution of average drop sizes obtained for Mixing II shows that larger drops are concentrated in the lower shear rate regions.

Keywords: Mixing; Liquids; Polymer processing; Drops

1. Introduction

The basic goal in mixing viscous immiscible fluids is to produce a mixture with a desired structure. The structure might be the morphology of a polymer blend or the drop size distribution of an emulsion. It is this structure which determines the final properties (and value) of the product, e.g. the rheology of shampoo or margarine in the consumer goods industry or the impact strength of a polymer blends in plastics manufacturing. Two links are crucial to this understanding—how mixing determines the structure and how the structure determines the properties. This work focuses on the link between process and structure.

Let us first consider a typical mixing process as it progresses from large to small scales (Fig. 1). The two materials are assumed to be Newtonian and liquid throughout the entire process. [In the case of polymers, the mixing process may start with unmelted solids and proceed through a melting stage which has been shown to have a significant effect on morphology (Sundararaj, Macosko, Rolando, & Chan, 1992); our viewpoint here, is obviously simplified.] In the beginning stages of mixing, large masses of the dispersed phase, d, are embedded in a continuous phase, c. The ratio of the viscosities of the dispersed to continuous phase μ_d/μ_c is denoted p.
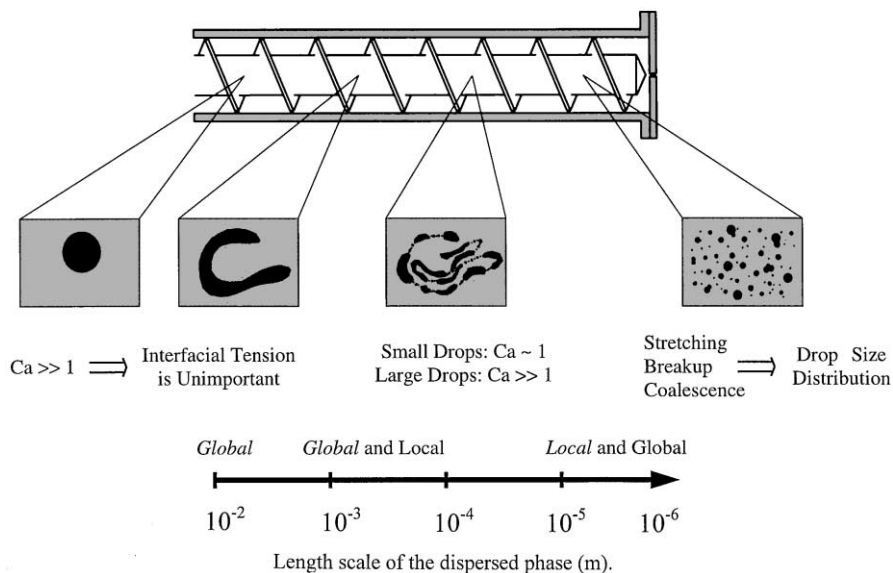
Fig. 1. Illustration of mixing immiscible liquids as the mixing process evolves from the initial stages in which mixing is controlled by the global properties of the flow—interfacial tension is unimportant—until the final stages in which the local processes of stretching, breakup, and coalescence control mixing.

The large masses of fluids are stretched and folded over. At this stage the capillary number, *Ca*, which is the ratio of the viscous forces to interfacial forces, is very large; therefore, interfacial forces do not play a significant role. As the process evolves, the capillary number decreases and the extended blobs break into many smaller drops. Concurrently, smaller drops begin to collide with each other and may coalesce into larger drops, which may in turn break again. The breakup and coalescence processes compete against each other and it is the result of this competition which determines the final drop size distribution or morphology.

The most common way to model the *initial stages* of mixing is to numerically solve the Stokes equations for the two phases. A number of methods, have been used for this purpose; the volume of fluid method (Zhang & Zumbrunnen, 1996; Chella & Viñals, 1996), moving mesh methods (Hyman, 1984), and the marker and cell technique (Chakravarthy & Ottino, 1996). Level set methods (Sussman et al., 1999), have not been used for mixing applications but they are well suited for this purpose as well. More recently, mapping methods have been developed; it may be possible to extend this methodology to multiphase systems as well (Wetzel & Tucker, 1999; Anderson, 1999; Kruijt, 2000). All methods work reasonably well for the beginning of mixing and each has its advantages depending on the problem being solved. All the methodologies, however, encounter computational limitations as the complexity of the problem increases. For example, the marker and cell technique involves placing marker particles at the interface between the two fluids and advecting the particles with the flow. As the length of the interface grows, marker particles must be added. In chaotic mixing, the stretching is exponential and so is the memory growth needed to track the growing interface. In addition, some of these methods may encounter difficulties when abrupt changes in the topology occur, such as in breakup or coalescence events.

Due to these computational limitations, there is currently no hope of solving a mixing problem in full from initial to final stages using the aforementioned techniques. A different, possibly scaled-down approach is needed. One possibility, zooming on the last stages of mixing, is to focus on the individual local processes that make up mixing: stretching, breakup, and coalescence. A great deal is known about each of these local processes, however, not every detail can be included or the model quickly becomes intractable. Therefore, the question becomes how to combine the most important physics of these local processes into a single tractable model.

A few attempts—for fluids and for solids—have been made in this direction. Manas-Zloczower, Nir, and Tadmor (1984) proposed a model for the dispersion of carbon black in an elastomer. The model essentially consists of repeatedly passing material through two zones; a high shear zone in which breakup of the agglomerates occurred and a low shear zone in which aggregation of the solids occurred to form larger agglomerates. By successively passing a distribution of solid particles through these zones, a final distribution of agglomerate sizes could be determined. A similar approach, for blending of highly viscous fluids, was taken by Janssen and Meijer (1995) and Huneault, Shi, and Utracki (1995).

2. Outline of this work

Two models are presented here: the first model (denoted *Mixing I* and presented in Sections 5 and 6) is suited for batch systems where decomposition into weak and strong flow regions is appropriate; the second model (*Mixing II*, presented in Sections 7 and 8) is suited for continuous flow systems and is intended to be used in conjunction with a fluid mechanical model of the flow. Model I augments the ideas presented by Janssen and Meijer (1995). The basic idea is to divide the mixer into two types of zones, strong and weak. The strong zone accounts for any stretching and breakup during flow that occurs during mixing, while the weak zone accounts for any coalescence and breakup that occurs at rest. Two new aspects are included: the formation of satellite drops and the distribution of stretching which arises in any real flow. In the Mixing II model, stretching and coalescence occur simultaneously depending on the local flow. Both models allow for observation of changes in the drop size distribution due to changes in material parameters (e.g. viscosities and interfacial tension) and process parameters (e.g. rotor speed in an internal mixer or flow rate in a continuous flow mixer).

Section 3 briefly discusses the nature of comparisons between computations and experiments—an issue that is central to the interpretation of the results presented here—whereas Section 4 presents the necessary fundamentals that go into both models. The three local processes; stretching, breakup, and coalescence, are briefly reviewed, highlighting the most important points (for a more complete review of the fundamentals see Ottino, De Roussel, Hansen, & Khakhar, 2000). Section 5 presents the basic computational procedure of Mixing I along with an application of the model to an idealized Banbury mixer (Sections 6 and 7). Sections 8 and 9 present the Mixing II model and its application to an idealized extruder. Section 10 concludes the paper by presenting results from both models and comparing trends, where possible, to experimental data from the literature.

3. Comparisons—computations/experiments

The goal of this work is to obtain an understanding of how different parameters in the processing step affect the final structure of a mixture. This understanding may be gained through computations and/or experiments and the results must be compared against each other. Computational predictions can be broken into three groups; (i) those which agree with experiments, (ii) those which disagree with experiments, and (iii) those with no comparable or companion experiments. Group (i) lends validity to the model, whereas (ii) and (iii) can potentially produce a higher level of understanding.

Comparisons which show disagreement between computations and experiments can often be reconciled either by looking at experiments from a different viewpoint or realizing that there is a fundamental piece of physics missing from the model. Resolving seemingly contradictory trends is what furthers understanding. Both, examples of using the models to help clarify experimental results and using experiments to suggest missing elements from the models are given in the results section.

Due to the flexibility of computations, a larger number of observations can be made using models rather than experiments. Therefore, some computational predictions may not have comparable experimental counterparts. Computations can therefore be used to probe unexplored areas of parameter space and suggest novel processing steps that may lead to desired properties in the final product. In this way computations can be used to guide experiments; an example of this, overemulsification, is given in a follow up paper (DeRoussel, Khakhar, & Ottino, 2001).

4. Fundamentals

4.1. Stretching of a drop

The degree of deformation and whether or not a drop breaks in a homogeneous flow is determined by the capillary number Ca, the viscosity ratio p, the flow type, and the initial drop shape and orientation. If Ca is less than a critical value, Ca_{crit}, the initially spherical drop is deformed into a stable ellipsoid. If Ca is greater than Ca_{crit}, a stable drop shape does not exist, and the drop is continually stretched until it breaks. All of the information, experiments and theory, known about the stability of a drop in a linear flow can be summarized in a plot Ca_{crit} vs. p, possibly with the flow type as a parameter (this was first obtained by Taylor, 1934). The first step in the model is to check if a drop will be deformed. It is important to stress that Ca_{crit} only gives the *maximum size drop that is stable in a given flow*, but does not say anything about the drop sizes produced upon breakup.

For $Ca_{crit} < Ca < \kappa Ca_{crit}$—with $\kappa \sim 2$ for simple shear flow and $\kappa \sim 5$ for elongational flow—stretching proceeds slowly (Janssen, 1993; Elemans, Bos, Janssen, & Meijer, 1993). For $Ca > \kappa Ca_{crit}$, the drop undergoes affine deformation in which the drop acts as a material element and is stretched into an extended cylindrical thread (this is apparent in the agreement between the computations and the experimental results of Tjahjadi & Ottino, 1991; see Fig. 6 in that paper).

4.2. Stretching and reorientations

Once the drop is deformed affinely, the *stretching rate and not the local shear rate* determines the amount of

distributive mixing. Simple shear flows give linear stretching and elongational flows give exponential stretching, however, it is difficult to achieve a sustained elongational flow in a practical mixer. The stretching rate in shear flows can be increased by incorporating periodic reorientations in the flow. The basic idea is to divide the flow into shorter sections with reorientations between each section. Consider an example. If a drop with a radius of 1000 μm is put through a total shear of 300 ($\dot{\gamma} = 50$ s^{-1} for 6 s), the length scale is reduced to 60 μm. If a reorientation is added after every 2 s, the length scale is reduced from 1000 to 1 μm. To get this same reduction without reorientation would take approximately 5.5 h, which is clearly longer than any practical mixing process should take. This idea is exploited in the example used in the Mixing II model.

The effect of reorientations—ubiquitous in mixing—must be taken into account. In complex flows, such as chaotic flows, as a fluid element travels through different regions of the flow, it experiences different amounts of stretching. If an assembly of fluid elements is considered at a given time, a distribution of stretching values is seen. One way to include this aspect is via stretching distributions (Muzzio, Swanson, & Ottino, 1992) which is the approach used in the Mixing II.

4.3. Breakup of drops

There are several possible mechanisms of drop deformation and breakup (for in depth reviews of breakup see Stone, 1994; Rallison, 1984; Acrivos, 1983; Eggers, 1997). For the types of flows considered here, the most important mechanism is capillary instability; in reality, however, more than one mechanism of breakup may be present. For example, close examination of the controlled mixing experiments pictures from Tjahjadi and Ottino (1991) shows the presence of three of the breakup mechanisms—necking, end-pinching, and capillary instabilities—as well as fold breakup, which is absent in homogeneous flows (Zhang, Zumbrunnen, & Liu, 1998). All mechanisms can be observed on different portions of the same extended thread, but capillary instabilities are dominant in mixing in polymer processing equipment (Meijer, Lemstra, & Elemans, 1988).

As discussed earlier, when $Ca > \kappa Ca_{\mathrm{crit}}$ a drop is stretched affinely and becomes a highly extended thread. The extended thread is unstable to minor disturbances and will eventually disintegrate into a number of large drops with smaller satellite drops between the large drops. The time for breakup of a thread—an important parameter in the model that must be calculated—depends on whether the thread is at rest or being stretched. For the case of a thread at rest, the initial growth of a disturbance can be relatively well characterized

by linear stability theory (Tomotika, 1935). However, the behavior eventually becomes non-linear which leads to the formation of the smaller satellite drops (Tjahjadi, Stone, & Ottino, 1992). Although linear stability theory does not predict the correct number and size of drops, the time for breakup, t_{break}, is reasonably estimated by the time for the fastest growing disturbance to reach half the average radius (Tomotika, 1935)

$$t_{\mathrm{break}} = \frac{2\mu_c R_0}{\sigma \Omega_m} \ln\left(\frac{0.82 R_0}{\alpha_0} \right), \qquad (4.1)$$

where μ_c is the viscosity of the continuous phase, σ is the interfacial tension, Ω_m is the non-dimensional growth rate which is a unique function of viscosity ratio and wavelength of the dominant disturbance, R_0 is the radius of the undisturbed thread, and α_0 is the initial amplitude of the disturbance. Kuhn (1953) estimated α_0 to be 10^{-9} m based on thermal fluctuations; Mikami, Cox, and Mason (1975) adopt a higher value (10^{-8}–10^{-7} m).

The distribution of drops produced upon breakup is dependent on the viscosity of the dispersed and continuous phases. Tjahjadi et al. (1992) examined the effect of varying the dispersed phase viscosity; they showed that the number of satellite drops increases as the dispersed phase viscosity decreases.

For the case of a thread breaking during flow, the analysis is complicated by the wavelength of each disturbance being stretched by the flow. This case was considered by Mikami et al. (1975), Khakhar and Ottino (1987) and Van Puyvelde, Yang, Mewis, and Moldenaers (2000). Mikami et al. (1975) and Khakhar and Ottino (1987) present a numerical scheme for determining t_{grow}, which is the time for the dominant disturbance to grow from α_0 to an amplitude equal to the average thread radius. The total breakup time, t_{break}, is the sum of t_{grow} and t_{crit}, where t_{crit} is the time to reach R_{crit} from R_0. The value of R_{crit} also comes out of the numerical scheme for calculating t_{grow}. Tjahjadi and Ottino (1991) used the numerical schemes for calculating R_{crit} and fit the results to the following equation:

$$R_{\mathrm{crit}} \approx (37.8 \pm 3.8)10^{-6} e_\lambda^{-0.89} p^{-0.44} \left(\frac{10^2 \sigma}{\mu_c \dot{\gamma}} \right)^{\chi}, \qquad (4.2)$$

where $0.84 < \chi < 0.92$ for $10^{-3} < p < 10^2$, e_λ is the mixing efficiency, and the units of the terms $\sigma/\mu_c\dot{\gamma}$ and R_{crit} are meters. The mixing efficiency e_λ is defined as

$$e_\lambda = \frac{\mathbf{D} : \mathbf{mm}}{(\mathbf{D} : \mathbf{D})^{1/2}}, \qquad (4.3)$$

where $\mathbf{m}$ is the orientation and $\mathbf{D} = \frac{1}{2}[\nabla \mathbf{u} + (\nabla \mathbf{u})^{\mathrm{T}}]$ with $\mathbf{u}$ being the velocity field (Ottino, 1989).

4.4. Coalescence of drops

As the process evolves drops begin to collide with each other and may coalesce. Coalescence is commonly pictured as consisting of three sequential steps; approach, drainage, and rupture. In reality, these three steps overlap somewhat. This view, however, provides a convenient way to model coalescence while capturing the most important physics. The most common approach in modeling collision is to use Smoluchowski's theory (see, for example Levich, 1962). This theory predicts the collision frequency, ω, for randomly distributed rigid spheres of equal size in simple shear flows without hydrodynamic interactions

$$\omega = \frac{4\dot{\gamma}\phi n}{\pi}. \tag{4.4}$$

Here ϕ is the volume fraction and n is the number of drops per unit volume. Eq. (4.4) gives at best an order of magnitude estimate for the collision frequency. However, it is important to note that, with the assumptions listed above, the collision frequency only varies by 5% for flows spanning from pure shear to pure elongation (Ottino et al., 2000). Therefore, we use Eq. (4.4) in the model to estimate the collision frequency of drops.

Once a collision occurs, the continuous liquid between the drops is squeezed into a film. As the drops are continually pushed together by the external flow field, the drops rotate as a dumbbell and the film drains. We use the approach of Chesters (1991) to model film drainage. The rate of drainage or approach, dh/dt, of the two drops separated by a distance h, is determined by the rigidity and mobility of the interface (the *mobility* of the interface depends on the viscosity ratio and determines the type of flow occurring during film drainage; the *rigidity* of the interface is a function of the interfacial tension and determines the amount a drop flattens during film drainage). Fig. 2 shows different expressions for dh/dt for various regimes.

The required time for complete film drainage is given by integrating the equations for dh/dt from h_0, the initial film thickness, to h_{crit}, the critical film thickness at which film drainage ends and rupture begins. The initial film thickness, h_0, is determined by setting dh/dt equal to the approach velocity at large separations. The driving force behind film drainage is not constant. The force varies as the drop doublet rotates according to the following equations (Allan & Mason, 1962):

$$F = 4.34\pi\mu_c R_0^2 \dot{\gamma} \sin 2\alpha, \tag{4.5}$$

$$\frac{d\alpha}{dt} = -\dot{\gamma}(0.8\cos^2\alpha + 0.2\sin^2\alpha), \tag{4.6}$$

where α is the collision angle (defined as the angle between the line tangent to the streamline on which a drop is moving and the line connecting the drop centers). The
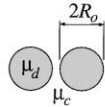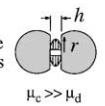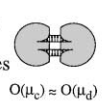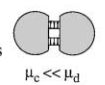

Fig. 2. Rate of drainage of the continuous film between two drops, dh/dt, is determined by the rigidity and mobility of the drops.

drainage time is obtained by integrating Eqs. (4.5) and (4.6) with the suitable equation of the set shown in Fig. 2.

Roughly speaking, if the mirror image of the initial collision angle is reached before the film thins to h_{crit}, the drops separate from each other. However, if h_{crit} is reached before then, the film ruptures and the drops coalesce. Rupturing of the film occurs when van der Waals forces become comparable to the driving force of film drainage. This generally occurs at thin spots, because van der Waals forces are inversely proportional to h^4 (Verwey & Overbeek, 1948). In general, the hole formation and rupture process occur on a much faster time scale than the film drainage. Coalescence is assumed to occur when h_{crit} is reached

$$h_{crit} = \left(\frac{AR}{8\pi\sigma}\right)^{1/3}, \tag{4.7}$$

where A is the Hamaker constant with a typical value of 10^{-20} J.

5. Mixing I: foundations and limitations

Let us now describe one way to integrate the elements described above into a single model. The basic idea of the Mixing I model is to divide a mixer into two typical types of zones, "strong" and "weak". In *strong zone* regions there is stretching and, possibly, breakup during stretching and in *weak zone* regions there is coalescence and breakup at rest. Exactly how the mixer is divided into zones depends upon the mixer—an example is given in Section 6. Once the "architecture" of the model is determined, an initial distribution of drops and/or threads is split into two parts (Fig. 3). One part of the distribution is sent to the weak zone and the other is sent to the strong zone. The distributions are passed through the zones
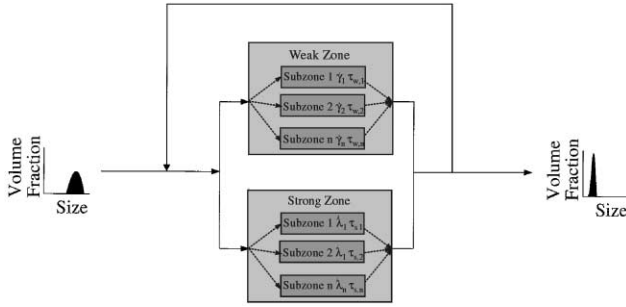
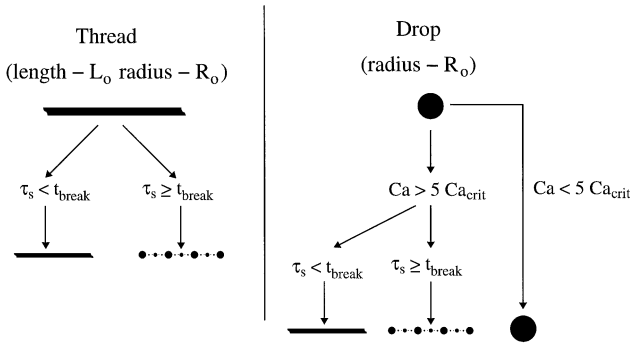Fig. 3. Basic architecture of the Mixing I model.

Fig. 4. Schematic of the computational procedure used in the Mixing I model for the strong zone.

and evolved according to the fundamentals outlined in Section 4.

5.1. Strong zones

The strong zone represents the regions of the mixer in which stretching and breakup during flow occurs. Distributions are generated by means of sub-zones; each sub-zone is characterized by its own stretching rate, shear rate, and residence time. Incoming drops to each sub-zone are checked to see if they can be deformed (Fig. 4)

$$Ca \geqslant \kappa Ca_{crit}. \qquad (5.1)$$

If this criterion is not met, the drop passes through the strong zone undisturbed. If this criterion is met *and* $\tau_s < t_{break}$, the drop is stretched into a thread according to

$$L = 2R_0 \exp(\dot{\lambda}\tau_s), \quad R = R_0 \exp(-\dot{\lambda}\tau_s), \qquad (5.1, 5.2)$$

where τ_s is the residence time in the strong zone and $\dot{\lambda}$ is the stretching rate. The time for the drop to break under flow is calculated from $t_{break} = t_{crit} + t_{grow}$, where t_{crit} is found using Eq. (4.2) and t_{grow} is estimated by $t_{grow} = 1.4/\dot{\gamma}$ (Janssen & Meijer, 1995). If the drop is able to break in the time allowed, $\tau_s \geqslant t_{break}$, the drop is replaced by the corresponding distribution of drops produced upon breakup. No work appears to have been reported on the distribution of drops produced for extended threads breaking during flow. Therefore, the

same distribution of satellite drops is used for both breakup during flow and breakup at rest. These drops are subsequently checked to see if they can be further stretched and broken, however, these drops only have time $\tau_s - t_{break}$ left in the strong zone. The same procedure is followed for each thread present, except the criterion for deformation does not have to be checked.

To account for the increase in viscous forces on a given drop due to the presence of surrounding drops relative to the viscous forces on a single drop surrounded by a pure continuous fluid, an effective viscosity is used in place of the continuous phase viscosity. The effective viscosity, $\mu_{c,eff}$, is only used in the deformation and stretching of drops and threads, but not in the film drainage stage where the presence of nearby drops is not necessarily felt. Following the approach of Janssen and Meijer (1995), we use a modified version of the Krieger and Dougherty (1959) equation,

$$\mu_{c,eff} = \mu_c \left(1 - \frac{\phi}{\phi_m}\right)^{-2.5\phi_m((p+0.4)/(p+1))}, \qquad (5.3)$$

where ϕ_m is the maximum packing density, which is a function of viscosity ratio and interfacial tension. Janssen and Meijer used a value of $\phi_m = 0.8$, which was based on a value close to $1 - \phi_{perc}$ where $\phi_{perc} \sim 0.156$ is the percolation threshold.

5.2. Weak zones

The weak zone represents the regions of the mixer where coalescence and breakup at rest occurs. As in the strong zone, the weak zone is divided into sub-zones to allow for a distribution of shear rates and residence times. The incoming distribution is split into parts and each part is sent to a separate sub-zone. Each sub-zone is stepped through in time, where the time step is $1/\omega$. At each time step the following steps are carried out (Fig. 5):

- Two drops are chosen at random from the drop array and placed in a collision array along with the time the collision occurred and the interaction (drainage or separation) time for these two particular drops, where the interaction time is calculated by integrating the suitable equations in Fig. 2.
- Each thread in the thread array is checked to see if it has been at rest long enough for breakup due to capillary instabilities to occur (see Eq. (4.1)). If enough time has elapsed for the thread to break, the thread is removed from the thread array and the corresponding distribution of drops is placed in the drop array. The distribution of drops used is based on the data given in Tjahjadi et al. (1992).
- The collision array is checked to see if any of the previous collisions have been interacting long enough for the film to drain to h_{crit} (see Eqs. (4.5–4.7)). If
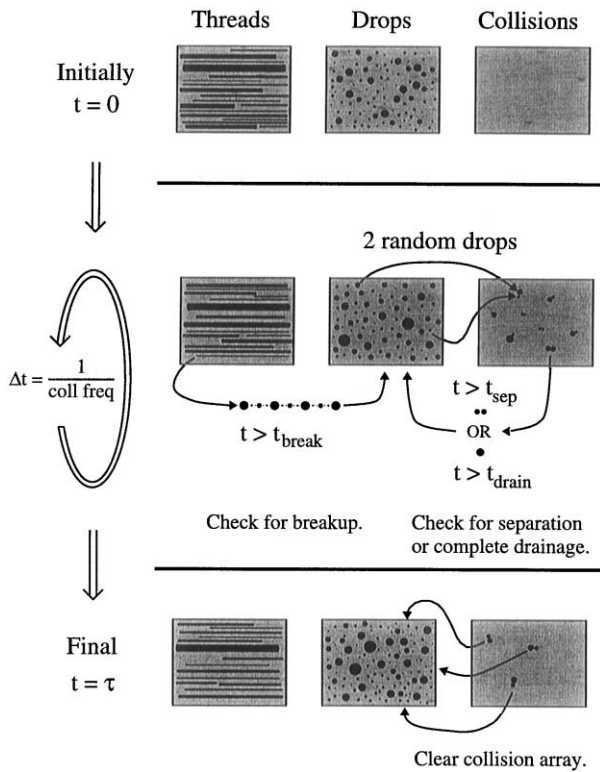
Fig. 5. Schematic of the computational procedure used in the Mixing I model for the weak zone.

this is the case, the two drops are removed from the collision array and a newly formed drop is placed in the drop array. However, if the mirror image of the initial collision angle is reached before the film thins to h_{crit}, then the two drops are separated and placed back in the drop array.

When the time in the weak zone reaches the residence time, all the drops in the collision array are separated and placed back in the drop array.

5.3. Limitations

The utility of the above computational procedure is limited by considerations of CPU time and computer memory. Using the above procedure requires that each individual drop and thread be tracked, which uses large amounts of memory. Consider a simulation with an initial condition of 1000 drops with an average size of 1000 μm. If the average size is reduced to 1 μm during the mixing process, then the total number of drops is 10^{12}. Assuming double precision variables are used (16 bytes each, this simulation would require less than 1 MB of memory initially, but 3×10^7 MB at the end. Also, if each drop is checked for deformation and each thread is checked for breakup the required CPU time quickly becomes unfeasible. To avoid this difficulty, the distribution of drops and threads is discretized and only the number of drops and

total length of threads of a given discrete size are tracked (Janssen & Meijer (1995) used the same approach).

A second problem occurs in the weak zone. For each collision, the suitable equations from Fig. 2 must be numerically integrated and extra memory must be allocated to keep track of how long the drops will interact with each other and the size of the drops generated. The number of collisions depends on the number of drops present. As mixing progresses and the number of drops increase, so does the number of collisions. Therefore, the required CPU time and computer memory quickly grows. Typical memory requirements to track collisions begin at less than 1 MB and increase to about 10^6 MB by the end of a simulation.

In order to avoid this problem, at the beginning of the weak zone, the number of drops is checked to see if a maximum limit has been exceeded. If this limit is exceeded, then the population of drops is "diluted"—that is, a representative sample of the overall distribution is chosen at random. The shape of the sample distribution is the same as that of the original distribution although the number of drops is reduced. It is the shape of the distribution that determines the accuracy. The coalescence routine is performed on this smaller distribution. At the end of the weak zone, the distribution is magnified so that volume is conserved.

6. Mixing I example: mixing in an idealized Banbury mixer

Internal batch mixers seem to be prime candidates for the strong–weak flow approach; regions of high shear between the wall and rotor and the regions of relatively low shear between the rotors. Rather than a full numerical simulation of the mixer using a flow simulation package, such as FIDAP, let us consider an idealized version of the mixer where all the necessary parameters (shear rate, stretching rates, and residence times) can be easily estimated. This allows us to focus on the dispersion aspects of the problem rather than the flow simulation and all the complications that go along with it. It should be noted, however, that complete flow simulations could be added later.

Consider an idealized Banbury mixer, where the strong zone is taken to be a small region around where the tip of the rotor approaches the wall and the weak zone is everywhere else (Fig. 6). The shear rate and residence time in the weak zone are estimated as

$$\dot{\gamma}_{\mathrm{weak}} = \frac{2\pi\Omega\bar{R}}{\bar{\delta}}, \quad \tau_{\mathrm{weak}} = \frac{V_{\mathrm{weak}}}{q}, \quad (6.4, 6.5)$$

where $\bar{R}$ is the average radial distance from the center to the edge of the rotor, $\bar{\delta}$ is the average gap between the wall and the rotor, Ω is the rotation rate of the rotor, q is the flow rate through the strong zone, and V_{weak} is the
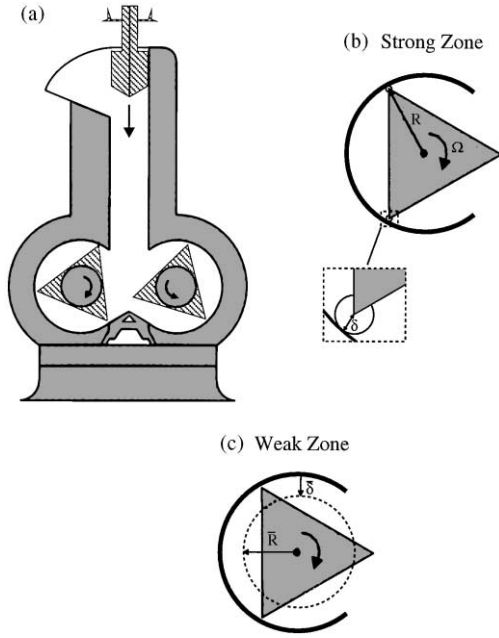
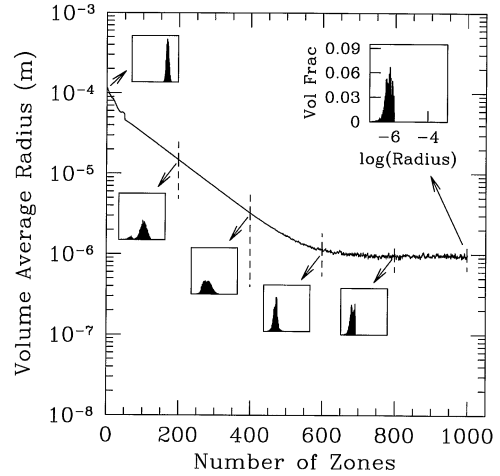Fig. 6. (a) Banbury internal mixer. Definition of the parameters for (b) the strong and (c) the weak zone.

Fig. 7. Typical results from the Mixing I model applied to a Banbury mixer. The volume average size of the dispersed phase is plotted versus the number of cycles through the zones. The actual distribution and vertical dashed lines representing the variance of the distribution at that point are also plotted ($\mu_c = 100$ Pa s, $\mu_d = 100$ Pa s, $\sigma = 5 \times 10^{-3}$ N/m, $\phi = 0.05$, and $\Omega = 50$ RPM).

volume of the weak zone. The shear rate and residence time in the strong zone are estimated as

$$\dot{\gamma}_{\text{strong}} = \frac{2\pi\Omega R}{\delta}, \quad \tau_{\text{strong}} = \frac{V_{\text{strong}}}{q}, \qquad (6.6, 6.7)$$

where R is the distance from the center to the tip of the rotor, δ is the gap between the rotor tip and wall, and V_{strong} is the volume of the strong zone.

The stretching rate in the strong zone is based on stretching calculations of Avalosse and Crochet (1997). They analyzed mixing in three 2D mixers: "three different systems—" single cam, corotating twin cam, and counter rotating twin cam. The flow was numerically solved and particle advection simulations were used to determine the stretching throughout the flow. Their results show that the length stretch increases exponentially with the number of rotations, i.e. $\lambda = \exp(2\pi\Omega t\beta)$, where $2\pi\Omega t$ gives the number of rotations and β is constant obtained form the numerical results. Therefore, the stretching rate is given by

$$\dot{\lambda} = 2\pi\Omega\beta. \qquad (6.8)$$

We use the case of corotating twin cams here.

The above approximations give a single value for residence times and shear rates. In order to produce a distribution, as a first approximation, the above values are assumed to be the mean value of normal distributions of shear rates and residence times. The parameters for each sub-zone are based on these distributions.

7. Mixing I: results and discussion

A typical simulation begins with splitting an initial distribution of drops into two parts and feeding them to the strong zone and to the weak zone. This distribution of drops is run through the computational procedure outlined in Sections 5.1 and 5.2. After each cycle (a single pass through both a strong and weak zone), the new distribution of drops is written to a file. The simulation continues until a steady state is reached.

In Figs. 7 and 8 the volume average and number average sizes are plotted versus the number of zones through which the distribution has been cycled, which is equivalent to time in the case of the Banbury mixer. Also shown is the standard deviation of the distribution—represented as the vertical dashed lines—and the actual distribution initially and after every 200 cycles through the strong and weak zones.

The averages and standard deviations of the drop size distribution are defined as

$$\text{Number:} \quad \bar{R}_n = \sum_{i=1}^{N} n_i R_i, \quad \sigma_n = \left[\sum_{i=1}^{N} n_i (R_i - \bar{R}_n)^2 \right]^{1/2}, \qquad (7.1, 7.2)$$

$$\text{Volume:} \quad \bar{R}_\phi = \sum_{i=1}^{N} \phi_i R_i, \quad \sigma_\phi = \left[\sum_{i=1}^{N} \phi_i (R_i - \bar{R}_\phi)^2 \right]^{1/2}, \qquad (7.3, 7.4)$$

where n_i and ϕ_i are the number fraction and volume fraction of drops of size i. For the remainder of the paper, the terms average size and standard deviation refer to *both*
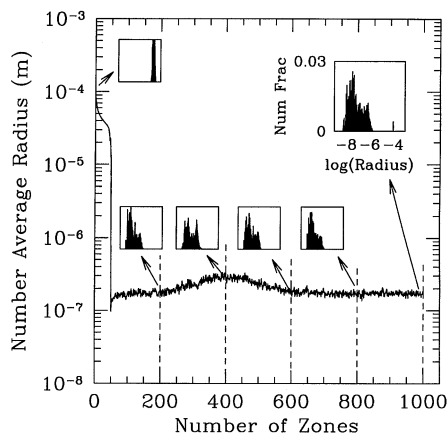
Fig. 8. Number average size of the dispersed phase is plotted versus the number of cycles through the zones. Same conditions as Fig. 7.

Fig. 9. Average size of the dispersed in a polymer blends made in Banbury mixers (—•— Favis & Chalifoux, 1987; —□— Schreiber & Olguin, 1983; —×— Tokita, 1976).

the number and volume based averages and standard deviations, unless explicitly stated that it is one or the other.

Consider the example illustrated in Fig. 7. Initially, $\bar{R}_\phi$ is approximately 100 μm. Once mixing begins $\bar{R}_\phi$ decreases exponentially as stretching and breakup dominate the process. As the size of the drops is reduced, coalescence begins to play a role and the average size levels off to a final value around 1 μm. At this point a dynamic equilibrium exists between stretching and breakup decreasing the average size and coalescence increasing the average size. The number average size shows a somewhat different behavior (Fig. 8). Shortly after mixing begins there is a sharp decrease in $\bar{R}_n$. This is where the first extended filament breaks into drops. After this breakup event occurs there are a large number of very small drops relative to the number of large drops. It is the large number of small drops which dominates $\bar{R}_n$. The volume average size, $\bar{R}_\phi$, does not go through this sharp decrease, because at this point it is dominated by the small number of large drops. Towards the end of mixing, $\bar{R}_n$ levels off to a final value as the dynamic equilibrium is established.

$\bar{R}_\phi$ and $\bar{R}_n$ are not the only averages. Another common average size, especially in the emulsion literature, is the Sauter mean diameter given by

$$R_{\text{Sauter}} = \frac{\sum_i 4\pi R_i^3/3}{\sum_i 4\pi R_i^2},\qquad(7.5)$$

where the sum is over all drops present. In fact, an infinite number of averages may be defined; the choice depends on the particular application. For example, if mass transfer between the phases is important, an average weighted by interfacial area would be the relevant average. It is important to remember, however, that different averages may display different behaviors, as demonstrated in Figs. 7 and 8. Therefore, it should be clearly stated to which average reference is being made. A few comments about the shape of the distributions should be made as well. In Fig. 7, the standard deviation is shown as the dashed
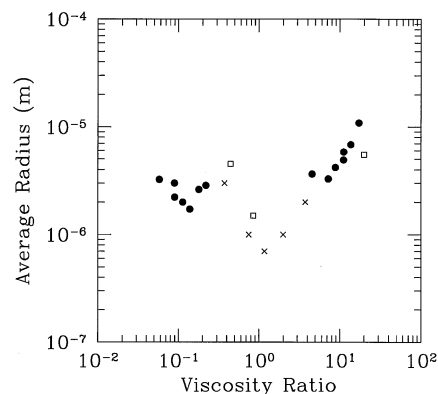
vertical lines. Notice that for in the number based case (Fig. 8) the lines below the average go off the scale, because the standard deviation is greater than the average. This is due to the distributions being skewed to the left. It is therefore apparent that the shape of the distribution is not completely characterized by the standard deviation. A more complete analysis requires other measures such as skewness and kurtosis.

A final issue is the role of randomness in the simulations. This arises due to the random selection of drops in the computational procedure for the weak zone in and the randomness in splitting the distribution which are sent to the strong and weak zone. These effects are, however, small. Consider a typical example: 10 simulations with the same set of parameters as those used for Fig. 7. These simulations give an average size of 0.96 μm with a standard deviation of 3.2×10^{-3} μm. It is apparent that there is a high degree of reproducibility in the simulations.

7.1. Viscosities

Fig. 9 shows three sets of experimental data obtained from the literature corresponding to a polymer blend produced in a Banbury mixer (Favis & Chalifoux, 1987; Schreiber & Olguin, 1983; Tokita, 1976). As is standard practice we plot the average size of the dispersed phase versus viscosity ratio. These data appear to show that the average size goes through a minimum as viscosity ratio is increased, and this seems to correspond to the trends of the classical Ca versus p plots. However, this is misleading.

Dimensional analysis shows that the actual values of *both* viscosities are important, rather than just the ratio of the two. In addition, these experiments have many other factors affecting the results, such as melting and elasticity. Sundararaj et al. (1992) have shown that a significant part of the size reduction in blending polymers occurs during the melting stage. Also, experiments from
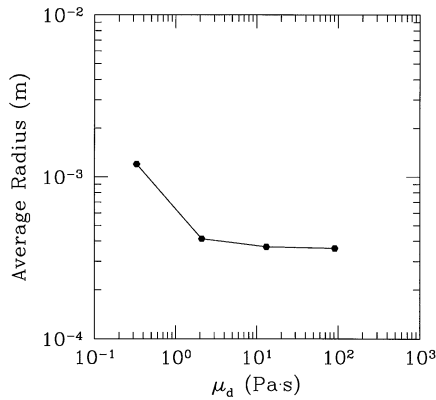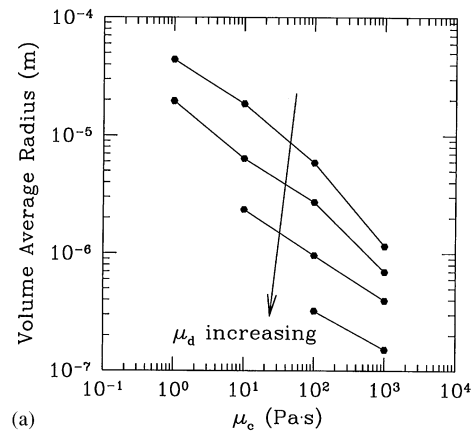
Fig. 10. Average size of the dispersed phase in a mixture of two immiscible Newtonian liquids in a controlled chaotic flow. Data from Tjajhadi and Ottino (1991). The experiment was done in a journal bearing apparatus at low volume fraction to avoid coalescence.

Sundararaj and Macosko (1995) show that the size of the dispersed phase may go through a minimum as rotor speed is increased. This behavior is attributed to elasticity acting as an additional restoring force on a drop. To get a better understanding of the role viscosities play in the mixing process it is convenient to consider a more basic experiment that is free from these extra factors.

Tjahjadi and Ottino (1991) conducted "pure breakup" experiments of Newtonian fluids (at very low volume fraction such that coalescence was negligible) in a journal bearing apparatus producing a controlled chaotic flow. In these experiments, a single continuous phase was kept constant and the dispersed phase was varied (Fig. 10). As the viscosity of the dispersed phase was increased, the average size decreased showing no minimum. The only variable in these experiments was the dispersed phase viscosity, so the extra factors present in the Banbury experiments were eliminated (however, the interfacial tension, which we assumed remained constant, was not measured).

This trend was examined with the Mixing I model (Fig. 11). When either viscosity was increased and the other was held constant, the volume average size decreased (Fig. 11a and b). This is in line with the results of Tjahjadi and Ottino (1991) (even though the flow fields are manifestly different). If the data from Fig. 11a and b are combined to examine the trend with viscosity ratio, the data becomes ambiguous—for a given viscosity ratio infinitely many different sizes are possible depending on the values of each individual viscosity (Fig. 12). The trends are the same if $\bar{R}_n$ is considered, except $\bar{R}_n$ is not as sensitive to μ_d. These trends can be explained by examining the roles of the local processes of stretching, breakup, and coalescence.

- *Stretching*: Increasing the continuous phase viscosity increases the viscous forces that act to deform a drop. Therefore, smaller drops can be deformed in a given

(a)
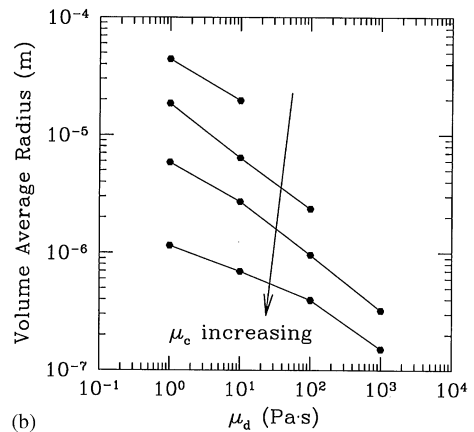
(b)

Fig. 11. Results from the Mixing I model for trends in volume average size of dispersed phase as viscosity is varied. Each line in (a) and (b) is for a constant dispersed and continuous phase viscosity, respectively. The arrows point in the direction of increasing viscosity (μ_c, $\mu_d = 1, 10, 100$, and 1000 Pa s, $\sigma = 5 \times 10^{-3}$ N/m, $\phi = 0.05$, and $\Omega = 50$ RPM).
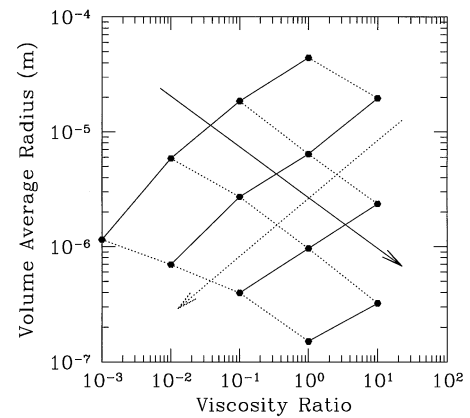

Fig. 12. The drop size data of Fig. 11 becomes ambiguous when plotted versus viscosity ratio. The solid and dashed lines represent constant dispersed and continuous phase viscosities, respectively, and the arrows point in the direction of decreasing viscosity ($\sigma = 5 \times 10^{-3}$ N/m, $\phi = 0.05$, and $\Omega = 50$ RPM).
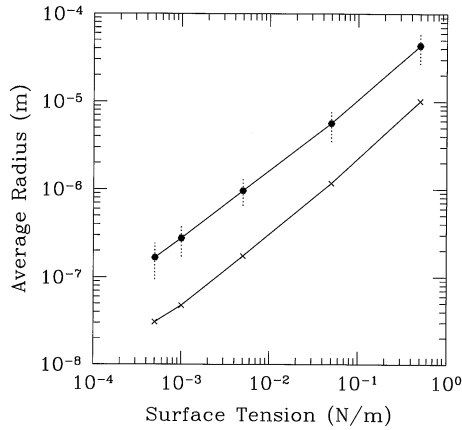
Fig. 13. Results from the Mixing I model for the trend in average size of the dispersed phase as interfacial tension is varied (—●— volume average size and —×— number average size). The vertical dashed lines represent the width of the distribution at that point ($\mu_c = 100$ Pa s, $\mu_d = 100$ Pa s, $\phi = 0.05$, and $\Omega = 50$ RPM).
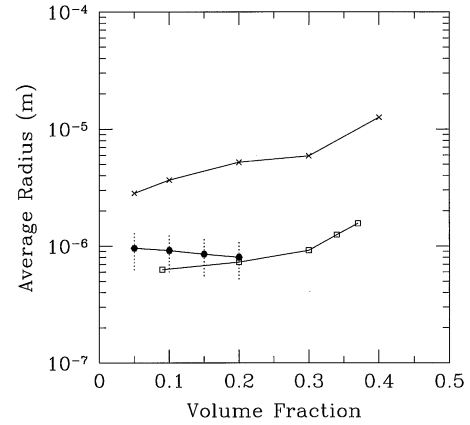

Fig. 14. Results from the Mixing I model (—●—) and experimental data (—□— Tokita, 1976 and —×— Favis & Chalifoux, 1988) for the trend in average size of the dispersed phase as volume fraction is varied. The vertical dashed lines represent the width of the distribution at that point ($\mu_c = 100$ Pa s, $\mu_d = 100$ Pa s, $\sigma = 5 \times 10^{-3}$ N/m, and $\Omega = 50$ RPM).

flow. However, the effect of Ca_{crit} must also be considered. Ca_{crit} may increase or decrease as the viscosities are changed depending on the viscosity ratio.

- *Breakup*: As either viscosity is raised breakup will be delayed. Therefore, the extended thread will be available for more stretching before breakup, which will result in smaller drops upon breakup.
- *Coalescence*: As either viscosity is raised the rate of film drainage decreases. Therefore, in a given amount of time, the maximum size drop which can coalesce decreases. This leads to smaller final drop sizes.

7.2. Interfacial tension

Simulations were done varying the interfacial tension and observing the changes in the drop distribution (Fig. 13). The average size increases with increasing interfacial tension, while the width of the distribution appears to be unaffected. The trend in the average size agrees with experiments from the literature (Wu, 1987; Plochocki, Dagli, & Andrews, 1990), however, there are no experimental data to compare with the width of the distribution. Based on the local processes, explanation of this trend is as follows:

- *Stretching*: Increased interfacial tension causes a decrease in Ca while Ca_{crit} remains constant. Therefore, an increase occurs for the minimum size drop that can be deformed in a given flow.
- *Breakup*: Increased interfacial tension results in a decrease in the time to breakup a given size thread. Therefore, larger threads can break in a given amount of time producing larger drops.
- *Coalescence*: Increased interfacial tension produces a more rigid drop. More rigid drops will not flatten as much during coalescence, so there is less film to drain

before rupture. A thinner film means less drainage time, so larger drops can coalesce in a given amount of time.

7.3. Volume fraction

It is generally accepted that an increase in the volume fraction of the dispersed phase will result in a larger average size of the dispersed phase. Two sets of experimental data (Tokita, 1976; Favis & Chalifoux, 1988) displaying this trend are shown in Fig. 14. However, when simulations were run at different volume fractions, the average size was virtually unaffected.

The trend (or lack thereof) from the simulations can be explained as follows:

- *Stretching*: Increasing the volume fraction produces an increase in the effective viscosity of the continuous phase. Due to this increase in effective viscosity smaller drops can be deformed in a given flow, which gives a smaller average drop size.
- *Coalescence*: Increasing the volume fraction produces an increase in the collision frequency. This in turn increases the number of coalescence events and results in a larger average size.

Because there is a disagreement between clear experiments and the simulations, it is apparent that there are certain key aspects missing from the model. In the model, the value for h_{crit} is taken to be a function of σ and R only. However, h_{crit} may also be dependent on ϕ, as suggested by Minale, Moldenaers, and Mewis (1997).

Another possibility is the effect nearby drops and threads have on the breakup process. Breakup of an isolated thread is caused by thermal fluctuations creating

disturbances on the surface of the thread that grow and eventually cause breakup. However, if nearby drops and threads create disturbances with different wavelengths and amplitudes, the distribution of drops produced upon breakup will be different from the case of an isolated thread. The sensitivity of the distribution of drops produced from a breakup event to the initial wavelength of the critical disturbance is considered by Tjahjadi et al. (1992). The value for α_0 in the simulation was taken to be a constant value of 10^{-9} m (Kuhn, 1953). If the disturbances are larger than that caused by thermal fluctuations, breakup will occur sooner (Tomotika's result) and produce larger drops. One possibility is that as the volume fraction of the dispersed phase is increased, the probability of a breakup event being influenced by nearby drops increases simply because more drops are present. A nice illustration of the influence of nearby threads on the breakup process is reported by Elemans, van Wunnik, and van Dam (1997). Their experiments show adjacent threads of nylon 6 in a polystyrene matrix breaking at rest. As the breakup process proceeds, the influence of nearby threads is apparent by the fact that the wavy surfaces of the threads are perfectly nested.

8. Mixing II: foundations and computational procedure

The Mixing I model is based on conceptually dividing a mixer into strong and weak zones. For a mixer such as a Banbury mixer, this approach works well; the tips of the rotor are taken as the strong zone and everywhere else is the weak zone. However, not all mixers allow for such a clear distinction. A second disadvantage of the Mixing I model is it does not capture distributive mixing. Fig. 15 exemplifies the possible problems. The figure shows an experiment in which a dispersed oil phase floats on a continuous phase of glycerine in a journal bearing apparatus (Swanson & Ottino, 1990). The initial condition (Fig. 15a) is a single large blob of the dispersed fluid. As mixing proceeds, the blob is stretched and broken into small drops (Fig. 15b and c) very much along the lines of the conceptual picture of Fig. 1. The steady-state result is shown in Fig. 15d, which shows a bimodal distribution of drops—one large drop and many small drops. Applying the Mixing I model for this case would (perhaps) predict the existence of a bimodal distribution (dispersive mixing), but it would not give any information about where the drops are in the mixer (distributive mixing).

Mixing II is not based on dividing mixers into zones, so it is applicable to a broader range of mixers. It uses particle advection simulations to obtain information about stretching rates, shear rates, and residence times throughout the mixer. The disadvantage, however, is that it requires substantially more computational power. At the moment of this research (*ca.* 1998) a typical simulation using Mixing I takes less than a day, whereas for Mixing
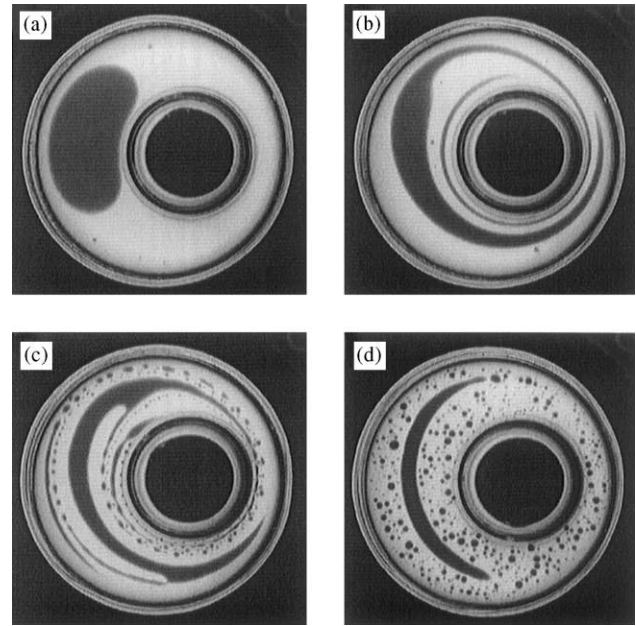

Fig. 15. Two-dimensional chaotic mixing experiments with colored silicone oil floating on glycerine. (a) Initial configuration, (b) and (c) intermediate configurations (d) final configuration.

II takes about a week. [These times correspond to simulations on an SGI Indigo2 with a 200 MHz R4400 processor and 384 MB of RAM (Spec Int 95 = 3.5 and Spec FP 95 = 3).]

8.1. Computational procedure

The coupling between local and global scales is obtained via particle advection simulations. Input information—stretching rates, shear rates, etc.—along with material parameters and initial conditions, yields as output the final drop distribution.

Consider, for example, an ideal single screw extruder, one described in terms of an approximate analytical solution. This significantly reduces the computational complexity of the particle advection step, thereby allowing the emphasis to be placed on the mixing aspects, rather than on the fluid mechanics. The flow is modeled by using the classical approximation (see for example Tadmor & Gogos, 1979) of unwinding the screw channel from the root of the screw (Fig. 16). The flow is viewed as flow through a straight channel with the top of the channel moving diagonally and a pressure flow in the negative z direction. The cross channel flow is modeled using the approach of Chella and Ottino (1985); obviously, several other approximations may be used. [Note that in describing the axial distance traveled in the above flow, there are two choices. The first is in the direction parallel with the axis of the screw (z_{screw}) and the second is the helical axis, which is the z-axis of the unwound channel (z_{chan}). These are related by $z_{\text{channel}} = z_{\text{screw}} \sin \theta$, where θ is the
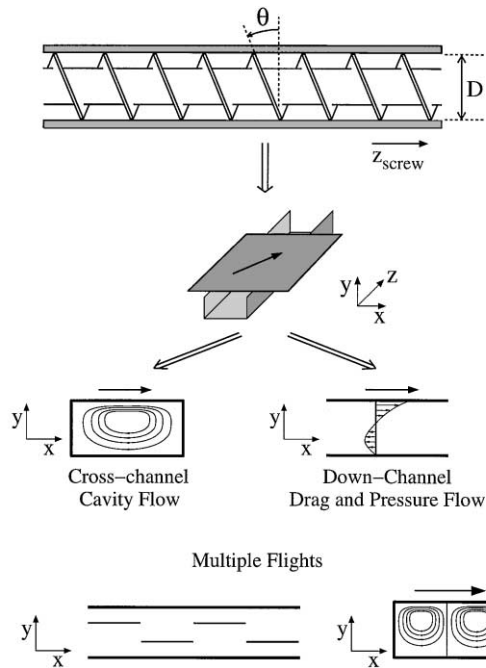
Fig. 16. The flow in a single screw extruder can be broken into a cross-channel and down-channel flow. Adding a second flight which extends the entire depth of the channel can be modeled by treating each side of the second flight as a separate channel.

Fig. 17. Sketch of the particle advection simulations.

helix angle. The length of extruders is commonly given in terms of a length to diameter ratio, where the length is measured parallel to the screw axis. This convention is followed here.]

The mixing is this flow is poor. The system is an example of a so-called duct flow, and therefore the stretching is linear (Franjione & Ottino, 1991). Improvements are possible. The *partitioned pipe mixer* (PPM) (Khakhar, Franjione, & Ottino, 1987) and *baffled cavity* (Jana, Tjahjadi, & Ottino, 1994) use changes in geometry to provide reorientations of the flow to generate exponential stretching. This effect can be created in our case by placing a second flight on the screw. In our idealized example, the second flight extends the full depth of the channel, so that the channel is divided into two smaller channels, and periodically changes position, as illustrated in bottom of Fig. 16. Fully developed flow is assumed in each of the two separate channels. Even though this is an idealized flow, the same principle may be used in practice [Tjahjadi & Foster (1996) and Jana, Scott, & Sundararaj (2000)—these extruders use a second flight which does not extend to the top of the channel and continually changes position].

8.2. Particle advection

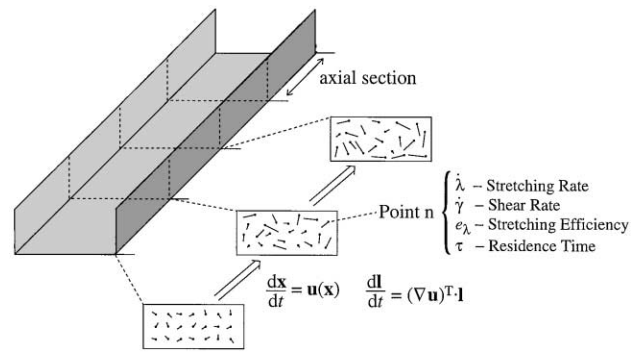The particle advection simulations are carried out using the same procedure used by developed by Swanson and Ottino (1990) and used by Hobbs and Muzzio (1997) for modeling mixing in the Kenics static mixer. Points are placed on a rectangular grid throughout a cross-section of the channel (Fig. 17). Each point is assigned a vector, $\mathbf{l}$, of unit length pointing in a random direction. The particles are advected and the vectors are stretched according to the following equations:

$$\frac{d\mathbf{x}}{dt} = \mathbf{u}(\mathbf{x}), \qquad \frac{d\mathbf{l}}{dt} = (\nabla\mathbf{u})^{\mathbf{T}} \cdot \mathbf{l}, \qquad (8.1, 8.2)$$

where $\mathbf{x}$ is the position of the point and $\mathbf{u}$ is the velocity. As particles pass a designated cross-section we note the following parameters assigned to each particle: average stretching rate, average mixing efficiency, average shear rate, and residence time.

8.3. Coalescence and breakup computational procedure

Once the particle advection step is completed, the first step in the Mixing II model is to randomly divide the initial distribution into a number of smaller distributions. Each passive particle is assigned one of these smaller distributions. The axial sections, which are the regions between the designated cross-sections, are stepped over in time. The time step is based on the minimum positive stretching rate. Note that if the stretching rate is small the amount of length stretch in an interval Δt is small. If the difference between the length at time t and the length at time $t + \Delta t$ is smaller than the size discretization used, the length stretch cannot be resolved. Therefore, a smaller size discretization or a larger time step is required. The time step is set according to the minimum stretching rate and the bin width of the size discretization

$$\Delta t = 2\frac{\ln(\text{bin width})}{\dot{\lambda}_{\min}}, \qquad (8.3)$$

where, Δt is the time step, $\dot{\lambda}_{\min}$ is the minimum stretching rate, bin width is the size of the bin in the size discretization, the factor of 2 being a "safety factor". An upper limit is placed on the time step, so that the time step will not be set by stretching rates which are essentially zero.
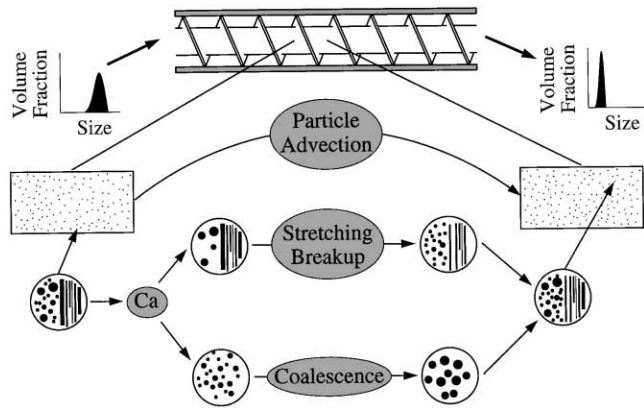
Fig. 18. Overview of the computational procedure used in the Mixing II model.
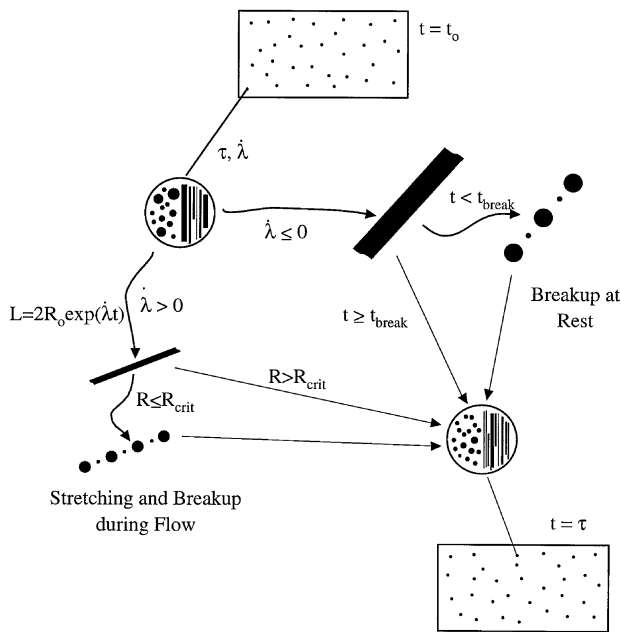

Fig. 19. Computational routine for stretching, breakup during flow, and breakup at rest.

At each time step drops are split into two groups, those that can stretch ($Ca > \kappa Ca_{crit}$) and those that cannot ($Ca < \kappa Ca_{crit}$) (see Fig. 18). The capillary number, Ca, is based on the local value of the shear rate, is obtained from the particle advection simulations. A sketch of the computational procedure for stretching and breakup is shown in Fig. 19. All threads, and those drops that can be stretched, are stretched according to Eqs. (5.1) and (5.2). If after stretching, the resulting thread has $R \leqslant R_{crit}$ [calculated from Eq. (4.2)], it will break into the corresponding distribution of drops. Threads which are not being stretched (those with $e_\lambda \leqslant 0$) are treated as threads at rest. These threads are checked to see if they have been at rest long enough for breakup to occur, $t \geqslant t_{break}$. In such a case, the thread is replaced by the corresponding distri-
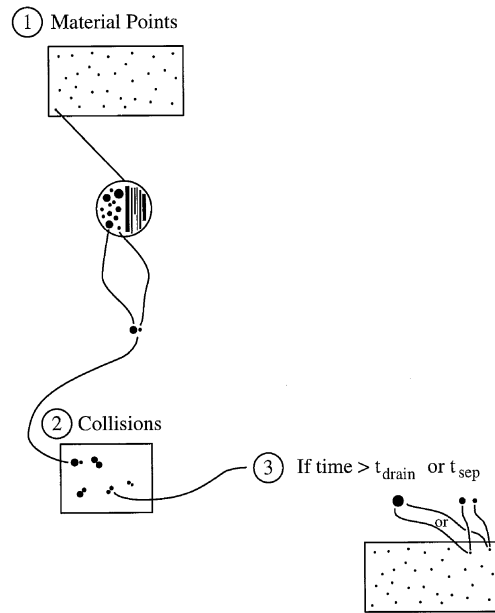

Fig. 20. Sketch of computational routine for coalescence for the Mixing II model.

bution of drops (and satellites). As in Mixing I, the drop size distributions corresponding to thread breakup at rest (Tjahjadi et al., 1992) are used.

The computational procedure for coalescence is as follows (Fig. 20). At each time step, n collisions occur, where n is the time step divided by the time between collisions. If the time between collisions is greater than the time step, then a collision does not occur at each time step. In this case, a collision occurs every i time steps, where i is the time between collisions divided by the time step.

For each collision, two drops are chosen at random. This drop pair is placed in a collision array along with the time of interaction during which the two drops will either separate or coalesce (calculated from the equations in Fig. 2). Also, at each time step all previous collisions are checked to see if enough time has elapsed for them to separate or coalesce $-t \geqslant t_{int}$. If this is the case, the drop pair is removed from the collision array and returned to the appropriate passive particle as a single drop if coalescence occurs or as two drops if separation occurs.

The same computational difficulties encountered in the first model are also encountered in this model. The distribution of drops and threads is discretized and only the total number of drops and the total length of threads of a given size are tracked. Also, the coalescence routine is only run on a sample of drops, due to the large amounts of memory and CPU time required to complete the calculations. After the coalescence routine is run the outlet distribution is readjusted to conserve volume.

One possible improvement on the above coalescence routine would be to allow the second drop chosen for the

collision pair to originate from either the same material point as the first drop or one of the nearest neighbors. However, there are some implementation problems. For illustrative purposes, consider a case with two material points each with a single drop. The drop on material point A stretches, but the drop on material point B does not. Eventually, the thread on point A breaks into a large number of small drops, but there is still only one large drop on point B. If the maximum number of allowable drops has been exceeded, a sample must be taken from each material point. The fraction of drops taken from each point must be the same. However, only one drop is on point B and a sample of a single drop cannot be taken. Therefore, the only way drops can collide with drops from the nearest neighbors, is if the sampling is not done. However, as discussed above, sampling is necessary or the model becomes intractable.

9. Mixing II: results and discussion

A typical simulation begins with randomly dividing the initial distribution of drops among the passive particles. Each of these smaller distributions is evolved according to the computational procedure outlined in the previous section. After each axial section the total distribution is written to a file. The simulation ends after the last axial section of the extruder is complete.

Fig. 21 shows the results from a typical simulation. The average size and the reciprocal of the average stretch are plotted versus the distance down the extruder. The distance down the extruder is given in terms of a length-to-diameter ratio where the length corresponds to the distance traveled parallel to the screw axis. Also shown is the actual drop distribution and the stretching distribution at regular intervals. Initially, the average size coincides with the reciprocal of the mean stretch, because mixing is dominated by stretching. The sharp decreases in both the mean stretch and the average size coincides with the change in position of the second flight. At the beginning of each secondary flight the stretching is higher because of the reorientations, so the average size also decreases at a higher rate.

At $z_{screw}/D \approx 7$, the average size begins to level off as the newly formed drops from breakup are too small to be deformed. Coalescence also becomes important which is apparent in the small increase in size over the length of each secondary flight. This is most apparent around $z_{screw}/D \approx 12$–14. At the beginning of each secondary flight the large drops formed from coalescence are reduced in size again.

Fig. 22 shows the change in the normalized standard deviation (standard deviation divided by the average size) over the length of the extruder. Also, shown is the average length stretch. Initially, the variance follows the average length stretch, but eventually it begins to deviate. The
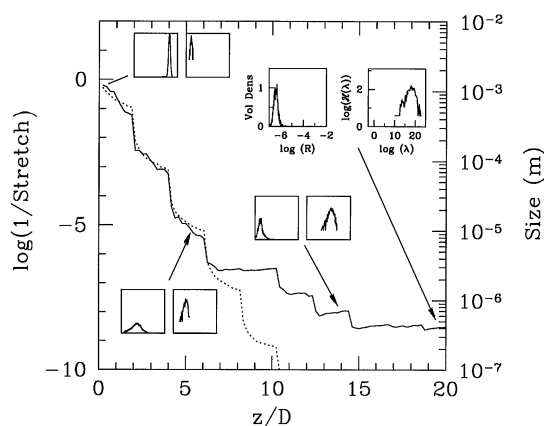

Fig. 21. Typical results from the Mixing II model applied to a single screw extruder. The average size (solid line) and reciprocal length stretch (dotted line) are plotted versus the distance down the extruder. Also shown as insets are the drop size and stretching distributions at regular intervals ($\mu_c = 100$ Pa s, $\mu_d = 100$ Pa s, $\sigma = 5 \times 10^{-3}$ N/m, and $\Omega = 60$ RPM).
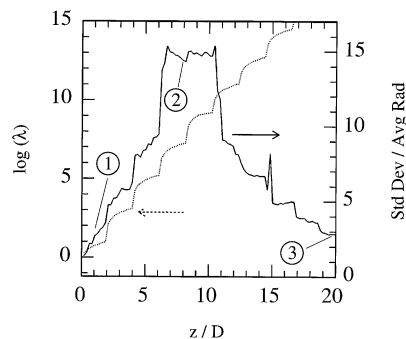

Fig. 22. Typical results from Mixing II applied to a single screw extruder. The normalized standard deviation (solid line) and length stretch (dotted line) are plotted versus the distance down the extruder. The numbers correspond to the those in Fig. 21 ($\mu_c = 100$ Pa s, $\mu_d = 100$ Pa s, $\sigma = 5 \times 10^{-3}$ N/m, and $\Omega = 60$ RPM).

variance reaches a maximum, decreases, and then begins to level off. The decrease in the variance occurs because the drops at larger sizes can still be stretched, but the smallest drops cannot. So, as illustrated in Fig. 23, the lower "bound" of the distribution does not move, but the upper bound does. This corresponds to a decrease in the variance.

9.1. Material parameters

The trends in the drop distributions as material parameters are varied produces the same results as the Mixing I model. Fig. 24a and b show the change in the volume average size as viscosities are varied. An increase in either viscosity causes a decrease in the average size. Plotting the data as a function of viscosity ratio shows that the average size is not a unique function of the viscosity ratio (Fig. 25). The trends can be explained in terms of
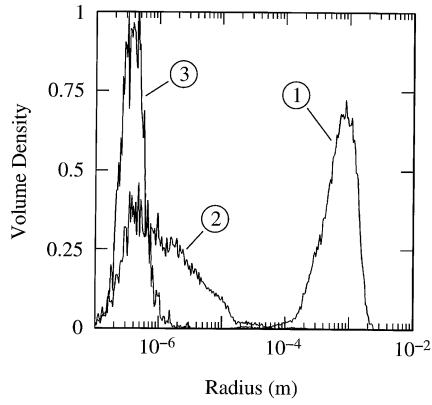
Fig. 23. Drop size distributions corresponding to the simulation of Fig. 22. The numbers correspond to those in Fig. 22.

Fig. 25. Data from Fig. 24 replotted as a function of viscosity ratio. Solid lines correspond to constant μ_c and dotted lines to constant μ_d.
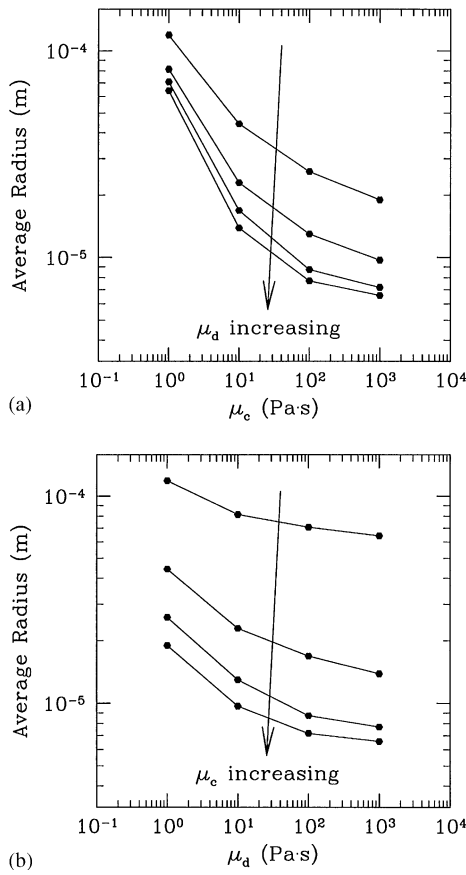

Fig. 24. Results from Mixing II for trends in volume average size as viscosity of the dispersed phase is varied. Lines correspond to (a) constant dispersed phase viscosity (b) constant continuous phase viscosity. Viscosity values used are μ_c, $\mu_d = 1, 10, 100, 1000$ Pa s ($\sigma = 5 \times 10^{-3}$ N/m, $\phi = 0.05$ and $\Omega = 60$ RPM).

Fig. 26. Results from Mixing II model for the trend in average size of the dispersed phase as surface tension is varied (—●— volume average size and —×— number size) ($\mu_c = 100$ Pa s, $\mu_d = 100$ Pa s, $\phi = 0.05$, and $\Omega = 60$ RPM).

stretching, breakup, and coalescence and it is the same way as for the Mixing I model (Section 3.2).

The trends in average size for changes in interfacial tension and volume fraction also match those of the Mixing I model. Fig. 26 illustrates that as interfacial tension
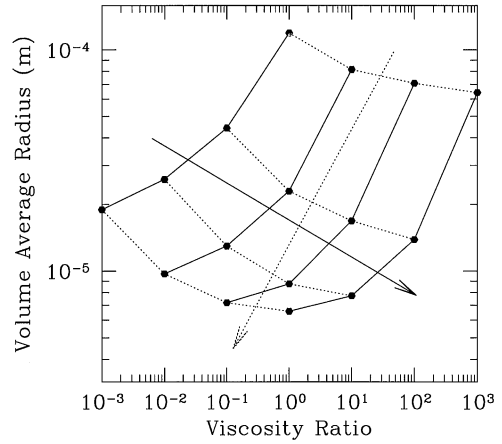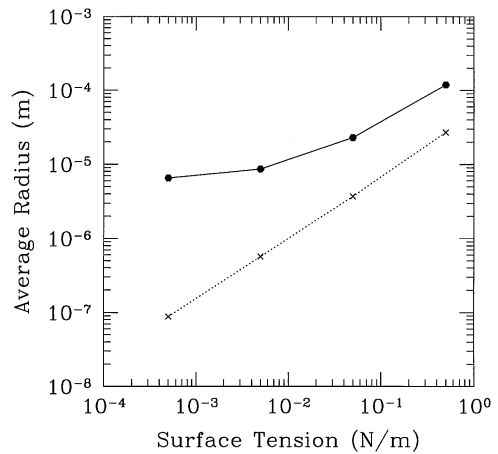
increases the average drop size increases. The trend in volume fraction is shown in Fig. 27. There is very little change in the average size as volume fraction varies. So, the same difficulty in accounting for the effect of volume fraction with the Mixing I model is encountered with the Mixing II model.

9.2. Fluid mechanical path

In order to examine the effect of the fluid mechanical path on mixing, simulations were run for extruders of the same total length but with different lengths of the secondary flight. By changing the length of the secondary flight, the stretching distribution changes, but the shear rate distribution does not. A decrease in the length of the secondary flight corresponds to an increase in the number of reorientations for an extruder of a given length. As
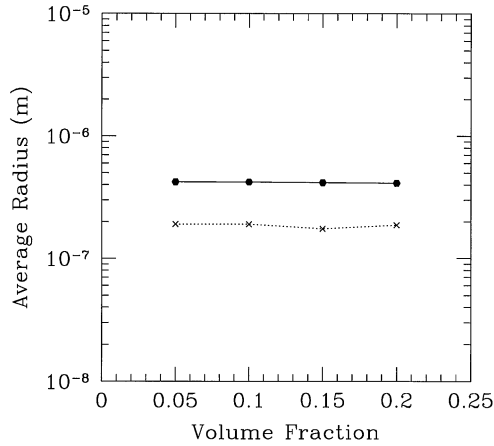
Fig. 27. Results from the Mixing II model for the trend in average size of the dispersed phase as volume fraction is varied (—●— volume average size and —×— number size) ($\mu_c = 100$ Pa s, $\mu_d = 100$ Pa s, $\sigma = 5 \times 10^{-3}$ N/m, and $\Omega = 60$ RPM).

Fig. 29. Results from the Mixing II model for the variation of the reciprocal of the length stretch for three different lengths of the secondary flight. Curve a: $l/D = 10$ (no reorientations) Curve b: $l/D = 2$ (5 orientations) Curve c: $l/D = 0.63$ (16 reorientations) ($\mu_c = 100$ Pa s, $\mu_d = 100$ Pa s, $\sigma = 5 \times 10^{-3}$ N/m, $\phi = 0.05$, and $\Omega = 60$ RPM).
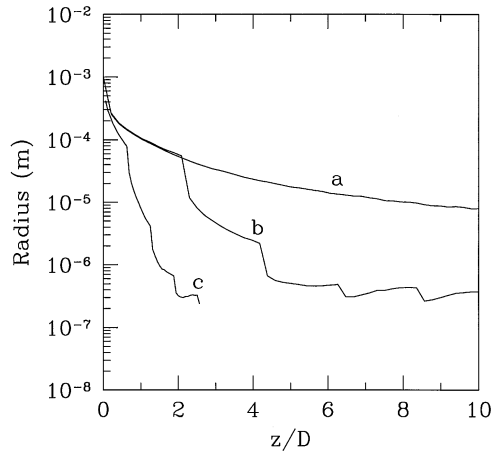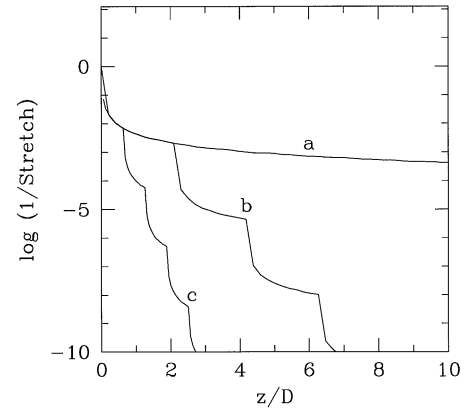

Fig. 28. Results from the Mixing II model for the variation of the average size for three different lengths of the secondary flight. Curve a: $l/D = 10$ (no reorientations) Curve b: $l/D = 2$ (5 orientations) Curve c: $l/D = 0.63$ (16 reorientations) ($\mu_c = 100$ Pa s, $\mu_d = 100$ Pa s, $\sigma = 5 \times 10^{-3}$ N/m, $\phi = 0.05$, and $\Omega = 60$ RPM).

illustrated in Fig. 28, adding reorientations gives higher stretching values. Three different lengths of the secondary flight are used (total extruder length, $L/D = 10$)

- $l/D = 10$ (one continuous flight) $\Rightarrow$ no reorientations
- $l/D = 2 \Rightarrow$ five reorientations
- $l/D = 0.63 \Rightarrow$ 16 reorientation

where, l is the length of the secondary flight.

Curve a in Fig. 28 shows the change in the volume average size over the length of the extruder (this should be compared with the reciprocal of the length stretch, shown in Fig. 29). The volume average size initially follows the reciprocal of the stretch (shown in Fig. 29), but begins to deviate as drops reach a size that can no longer be deformed. For the case where no reorientations occur, the drop distribution never reaches a steadystate as it does for the case of five reorientations and 16 reorientations.

For the case of 16 reorientations the steady state is reached the fastest, but the steady-state size is the same as for the case with five reorientations. Therefore, no benefit comes with the extra reorientations for a given extruder. In reality, there is an energy cost associated with each reorientation. More reorientations require a higher input of energy, so the extra reorientation would actually be a detriment rather than a benefit. Based on this there must be optimum number of reorientations. For the case presented in Fig. 28, the optimum appears to be five reorientations, because the distribution levels out right at the end of the extruder. For 16 reorientations, the final size is reached early on and subsequent reorientations do no provide any additional benefit.

Much can be done to correlate the results—e.g. distribution of average sizes at the exit cross-section—with fluid mechanical-based parameters, such as the distribution of exit times and shear rates. Only one example is shown here. Fig. 30 shows the distribution of shear rates in the system of Fig. 16; when this distribution is compared with the distribution of drop sizes over the cross-section is it seems that large droplets are more prevalent in the narrow channel. This can be rationalized easily: coalescence is more likely to occur at lower shear rates.

10. Summary

Mixing I is based on breaking a mixer into zones and evolving drop distributions within these zones according to the fundamentals of stretching, breakup, and
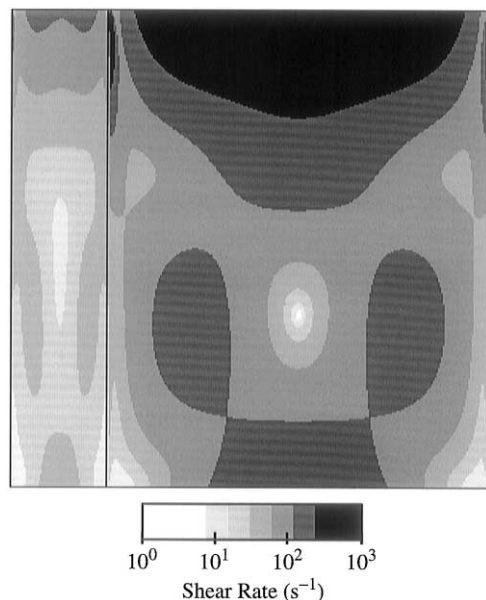
5528

Fig. 30. Shear rate distribution across the channel of the extruder. In general, the narrow part of the channel has a lower shear rate than the wide part of the channel. Therefore, coalescence is more likely in this region ($\Omega = 60$ RPM).

coalescence. Two aspects included in the model, which had not been considered before are the distribution of satellite drops produced from breakup of an extended liquid thread and the distribution of stretching values present in complex flows.

The division of a mixer into zones is a key assumption upon which the current Mixing I model is based. The mixer used as an example here, the Banbury mixer, is broken into zones relatively easily—in fact, many batch systems fall in this category. A natural question to ask is what can be done to model other types of mixers where the division into zones is not as clear, e.g. extruders. Mixing II does not rely on this assumption and it is more flexible in the sense that it applies to a broader range of mixer. Mixing II also yields information of the spatial distribution of drops in the mixer, which is not possible for Mixing I. However, Mixing II is more computationally intensive than Mixing I model, because it relies on particle advection simulations. Trends obtained from Mixing II are similar to those obtained from Mixing I.

The results from Mixing I were compared to experiments from the literature. Some of these comparisons—trends in the average size of the dispersed phase as interfacial tension was varied—agreed with published data. Others seemingly disagreed, but were reconciled by looking at the experiments in a different way. It was pointed out that considering trends in average size as a function of viscosity ratio is incorrect. Yet, there were model predictions which could not be compared with experiments; overemulsification falls in this category (DeRoussel et al., 2001).

References

Acrivos, A. (1983). The breakup of small drops and bubbles in shear flows. *Fourth international conference on physicochemical hydrodynamics. Annual New York Academy of Sciences, 404*, 1–11.

Allan, R. S., & Mason, S. G. (1962). Particle motion in sheared suspensions—XIV. Coalescence of liquid drops in electric and shear fields. *Journal of Colloid Interface Science, 17*, 383–408.

Anderson, P. D. (1999). *Computational analysis of distributive mixing.* Ph.D. thesis, Eindhoven University, The Netherlands.

Avalosse, Th., & Crochet, M. J. (1997). Finite element simulation of mixing: 1. Two-dimensional flow in periodic geometry. *A.I.Ch.E. Journal, 43*, 577–587.

Chakravarthy, V. S., & Ottino, J. M. (1996). Mixing of two viscous fluids in a rectangular cavity. *Chemical Engineering Science, 51*, 3613–3622.

Chella, R., & Ottino, J. M. (1985). The fluid mechanics of mixing in a single screw extruder. *Industrial and Engineering Chemistry, Fundamentals, 24*, 170–180.

Chella, R., & Viñals, J. (1996). Mixing of a two phase fluid by cavity flow. *Physics Review E, 53*, 3832–3840.

Chesters, A. K. (1991). The modeling of coalescence processes in fluid-liquid dispersions: A review of current understanding. *Transactions of the Institution of Chemical Engineers, 69*, 259–270.

DeRoussel, P., Khakhar, D.V., & Ottino, J.M. (2001). Mixing of viscous immiscible liquids. Part 2: Overemulsification—interpretation and use. *Chemical Engineering Science, 56*(19), 5531–5537.

Eggers, J. (1997). Nonlinear dynamics and breakup of free surface flows. *Reviews in Modern Physics, 69*, 865–930.

Elemans, P. H. M., Bos, H. L., Janssen, J. M. H., & Meijer, H. E. H. (1993). Transient phenomena in dispersive mixing. *Chemical Engineering Science, 48*, 267–276.

Elemans, P. H. M., van Wunnik, J. M., & van Dam, R. A. (1997). Development of morphology in blends of immiscible polymers. *A.I.Ch.E. Journal, 43*, 1649–1651.

Favis, B. D., & Chalifoux, J. P. (1987). The effect of viscosity ratio on the morphology of polypropylene/polycarbonate blends during processing. *Polymer Engineering Science, 27*, 1591–1600.

Favis, B. D., & Chalifoux, J. P. (1988). Influence of composition on the morphology of polypropylene/polycarbonate blends. *Polymer, 29*, 1761–1767.

Franjione, J. G., & Ottino, J. M. (1991). Stretching in duct flows. *Physics of Fluids A, 3*, 2819–2821, 1991; *erratum* (1994). *Physics of Fluids, 6*, 3501.

Hobbs, D. M., & Muzzio, F. J. (1997). The Kenics static mixer: A three-dimensional chaotic flow. *Chemical Engineering Journal, 67*, 153–166.

Huneault, M. A., Shi, Z. H., & Utracki, L. A. (1995). Development of polymer blend morphology during compounding in a twin-screw extruder. Part IV: A new computational model with coalescence. *Polymer Engineering Science, 35*(1), 115–127.

Hyman, J. M. (1984). Numerical methods for traking interfaces. *Physica D, 12*, 396–407.

Jana, S. C., Scott, E. W., & Sundararaj, U. T. (2000). *Single extruder screw for efficient blending of miscible and immiscible polymeric materials.* US Patent No. 6,132,076.

Jana, S. C., Tjahjadi, M., & Ottino, J. M. (1994). Chaotic mixing of viscous fluids by periodic changes in geometry—baffled cavity flow. *A.I.Ch.E. Journal, 40*, 1769–1781.

Janssen, J. M. H. (1993). *Dynamics of liquid–liquid mixing.* Ph.D. Thesis, Eindhoven University of Technology.

Janssen, J. M. H., & Meijer, H. E. H. (1995). Dynamics of liquid–liquid mixing: A 2-zone mixing model. *Polymer Engineering Science*, 35, 1766–1780.

Khakhar, D. V., & Ottino, J. M. (1987). Breakup of liquid threads in linear flows. *International Journal of Multiphase Flow*, 13(1), 71–86.

Khakhar, D. V., Franjione, J. G., & Ottino, J. M. (1987). A case study of chaotic mixing in deterministic flows: The partitioned pipe mixer. *Chemical Engineering Science*, 42, 2909–2926.

Krieger, I. M., & Dougherty, T. J. (1959). A mechanism for non-Newtonian flow of suspensions of rigid spheres. *Transactions of the Society of Rheology*, 3, 137–152.

Kruijt, P. (2000). *Analysis and optmization of laminar mixing: Design, development and application of the mapping method.* Ph.D. thesis, Eindhoven University, The Netherlands.

Kuhn, W. (1953). Spontane Aufteilung von Flussigkeitszylindern in Klein Kugeln. *Kolloid Zornal*, 132, 84–99.

Levich, V. G. (1962). *Physicochemical hydrodynamics*. Englewood Cliffs, NJ: Prentice-Hall.

Manas-Zloczower, I., Nir, A., & Tadmor, Z. (1984). Dispersive mixing in rubber and plastics. *Rubber Chemical Technology*, 57, 583–620.

Meijer, H. E. H., Lemstra, P. J., & Elemans, P. M. H. (1988). Structured polymer blends. *Makromolekulare Chemical Makromolekulare Symposia*, 16, 113–135.

Mikami, T., Cox, R. G., & Mason, S. G. (1975). Breakup of extending liquid threads. *International Journal of Multiphase Flow*, 2, 113–138.

Minale, M., Mewis, J., & Moldenaers, P. (1997). Effect of shear history on the morphology of immiscible polymer blends. *Macromolecules*, 30, 5470–5475.

Muzzio, F. J., Swanson, P. D., & Ottino, J. M. (1992). Mixing distributions produced by multiplicative stretching in chaotic flows. *International Journal of Bifurcation and Chaos*, 2(1), 37–50.

Ottino, J. M. (1989). *The kinematics of mixing: Stretching, chaos and transport*. Cambridge, UK: Cambridge University Press.

Ottino, J. M., DeRoussel, P., Hansen, S., & Khakhar, D. V. (2000). Mixing and dispersion of viscous liquids and powdered solids. *Advances in Chemical Engineering*, 25, 105–204.

Plochocki, A. P., Dagli, S. S., & Andrews, R. D. (1990). The interface in binary mixtures of polymers containing a corresponding block copolymer: Effects of industrial mixing processes and of coalescence. *Polymer Engineering Science*, 30, 741–752.

Rallison, J. M. (1984). The deformation of small viscous drops and bubbles in shear flows. *Annual Reviews in Fluid Mechanic*, 16, 45–66.

Schreiber, H. P., & Olguin, A. (1983). Aspects of dispersion and flow in thermoplastic-elastomer blends. *Polymer Engineering Science*, 23, 129–134.

Stone, H. A. (1994). Dynamics of drop deformation and breakup in viscous fluids. *Annual Reviews in Fluid Mechanics*, 26, 65–102.

Sundararaj, U., & Macosko, C. W. (1995). Drop breakup and coalescence in polymer blends: The effects of concentration and compatibilizers. *Macromolecules*, 28, 2647–2657.

Sundararaj, U., Macosko, C. W., Rolando, R. J., & Chan, H. T. (1992). Morphology development in polymer blends. *Polymer Engineering Science*, 32, 1814–1823.

Sussman, M., Almgren, A. S., Bell, J. B., Colella, P., Howell, L. H., & Welcome, W. L. (1999). An adaptive level set approach for incompressible two-phase flows. *Journal of Compounds*, 148, 81–124.

Swanson, P. D., & Ottino, J. M. (1990). A comparative computational and experimental study of chaotic mixing of viscous fluids. *Journal of Fluid Mechanics*, 213, 227–249.

Tadmor, Z., & Gogos, C. G. (1979). *Principles of polymer processing*. New York: Wiley.

Taylor, G. I. (1934). The formation of emulsions in definable fields of flow. *Proceedings of the Royal Society of London*, A143, 501–532.

Tjahjadi, M., & Foster, R. W. (1996). Single screw extruder capable of generating chaotic mixing. US patent. 5, 551,777.

Tjahjadi, M., & Ottino, J. M. (1991). Stretching and breakup of droplets in chaotic flows. *Journal of Fluid Mechanics*, 232, 191–219.

Tjahjadi, M., Stone, H. A., & Ottino, J. M. (1992). Satellite and subsatellite formation in capillary breakup. *Journal of Fluid Mechanics*, 243, 297–317.

Tokita, N. (1976). Analysis of morphology formation in elastomer blends. *Rubber Chemical Technology*, 50, 292–300.

Tomotika, S. (1935). On the instability of a cylindrical thread of a viscous liquid surrounded by another viscous fluid. *Proceedings of the Royal Society*, A150, 322–337.

Van Puyvelde, P., Yang, H., Mewis, J., & Moldenaers, P. (2000). Breakup of filaments in blends during simple shear flow. *Journal of Rheologhy*, 44, 1401–1415.

Verwey, E. J., & Overbeek, J. T. G. (1948). *Theory of the stability of lyophobic colloids*. Amsterdam: Elsevier.

Wetzel, E. D., & Tucker, C. L. (1999). Area tensors for modeling microstructure during laminar liquid–liquid mixing. *International Journal of Multiphase Flow*, 25, 35–61.

Wu, S. (1987). Formation of dispersed phase in incompatible polymer blends: Interfacial and rheological effects. *Polymer Engineering Science*, 27(5), 335–343.

Zhang, D. F., & Zumbrunnen, D. A. (1996). Influences of fluidic interfaces on the formation of fine scale structures by chaotic mixing. *Journal of Fluids Engineering*, 118, 40–47.

Zhang, D. F., Zumbrunnen, D. A., & Liu, Y. H. (1998). Morphology development is shear flow of straight and folded molten fibers. *A.I.Ch.E. Journal*, 44, 442–451.